frontiers | Frontiers in Materials

TYPE Original Research
PUBLISHED 10 January 2023
DOI 10.3389/fmats.2022.1099997

Check for updates

OPEN ACCESS

EDITED BY
Yinlong Zhang,
University of Chinese Academy of Sciences, China

REVIEWED BY
Junchao Xu,
University of Pennsylvania, United States
Yujun Song,
Nanjing University, China

*CORRESPONDENCE
Li Xu,
xuli@jlu.edu.cn
Yi Guo,
guoyi@jlu.edu.cn

†These authors have contributed equally to this work and share first authorship

SPECIALTY SECTION
This article was submitted to Smart Materials, a section of the journal Frontiers in Materials

RECEIVED 16 November 2022
ACCEPTED 05 December 2022
PUBLISHED 10 January 2023

CITATION
Zhang X, Yan Q, Wang J, Xu L and Guo Y (2023), The antitumor activity of Bax BH3 peptide delivered by gold nanoparticles.
Front. Mater. 9:1099997.
doi: 10.3389/fmats.2022.1099997

COPYRIGHT
© 2023 Zhang, Yan, Wang, Xu and Guo. This is an open-access article distributed under the terms of the Creative Commons Attribution License (CC BY). The use, distribution or reproduction in other forums is permitted, provided the original author(s) and the copyright owner(s) are credited and that the original publication in this journal is cited, in accordance with accepted academic practice. No use, distribution or reproduction is permitted which does not comply with these terms.

The antitumor activity of Bax BH3 peptide delivered by gold nanoparticles

Xi Zhang†, Qi Yan†, Jingying Wang, Li Xu* and Yi Guo*

Key Laboratory for Molecular Enzymology and Engineering, The Ministry of Education, National Engineering Laboratory for AIDS Vaccine, School of Life Sciences, Jilin University, Changchun, China

Cancer has long remained one of the primary causes of disease and death globally, and it continues to pose a significant threat to human health. Surgery, radiotherapy, and chemotherapy are traditional treatments for cancer which are still widely used. However, while both surgery and radiotherapy remain acceptably effective in addressing a variety of primary tumors, neither possesses therapeutic potential for unknown metastatic lesions which may exist elsewhere in the patient's body. Conversely, while systemic chemotherapy does have the potential for therapeutic efficacy on both primary and metastatic lesions alike, drug targeting is often poor, side effects are typically high, and treatment efficacy is still often lacking. Nanomedicine presents a promising solution to the above issues. For example, nanocarriers can be used to increase drug selectivity and targeting, increasing efficacy and decreasing side effects. Based on the role of the lethal domain of Bcl-2 family proteins, which play roles in apoptosis, the BH3-only protein, a section of BH3 peptide with a sequence of Asp-Ala-Ser-Thr-Lys-Lys-Leu-Ser-Glu-Cys-Leu-Arg-Arg-Ile-Gly-Asp-Glu-Leu-Asp-Ser. However, treatments based on soluble BH3 peptides, as with those based on other biologically active macromolecules, exhibit low cell membrane permeability, poor stability against proteolysis, and low endosomal escape rates. In this paper, attempt to address these issues by developing a variety of BH3@gold nanoparticle drug systems with different coating ratios. We demonstrate, high loading efficiency and, excellent anti-tumor effects *in vitro*, including inhibition of proliferation and migration in the human lung adenocarcinoma cell line, A549. Our results present a new possibility for anticancer peptide drugs in the future.

KEYWORDS

cancer, nanomedicine, BH3 peptide, tumor therapy, gold nanoparticle

1 Introduction

Cancer is a leading cause of death worldwide, and it is estimated that more than 21 million people could be living with cancer by 2030 (Allemani et al., 2018; Chen et al., 2018). So far, a variety of treatment methods including surgical resection, chemotherapy, molecular targeted therapy, gene therapy, radiotherapy, immunotherapy, and photothermal therapy have been widely used in the clinical treatment of cancer (Zou

et al., 2016; Lee et al., 2018; Li et al., 2021; Yahya and Alqadhi, 2021), but there are serious adverse reactions associated with each of these, including high systemic toxicity, high probability of metastasis, and severe organ damage. In recent decades, nanomedicine, a branch of nanotechnology, has made great contributions in the diagnosis, imaging, and treatment of cancer, providing researchers and clinicians with new research tools for addressing this ubiquitous disease. Nanomedicine refers to the use of nanoscale or nanostructured materials in medicine, including at least one structure with a characteristic size up to 300 nm (Etheridge et al., 2013). Since the first clinical application of nanomedicines in the 1980s, several new nanomedicines have been officially approved and marketed in the European Union, United States, and Japan (Wang et al., 2018). For example, Ling et al. self-assembled P6NPs nanoparticles, which were shown to reduce the toxicity of cisplatin on the liver and kidney in nude mice, and further to promote apoptosis of tumor cells through glutathione elimination in these mice, thus reducing their overall systemic toxic and side effects (Ling et al., 2019). Xu et al. (2019); Zhang and Liu, 2019) developed a simple strategy to change the natural properties of siRNA with high molecular weight, negative charge, and hydrophilicity inherent properties by simply mixing it with doxorubicin to form a hydrophobic complex, so that it can be encapsulated in non-cationic PEG-polylactic acid (PLA) micelles for whole-body delivery. It is known clear that nanomedicine has many advantages, such as 1) Improving the water solubility and delivery efficiency of drugs in the body; 2) Improving the targeting of drugs to promote their accurate delivery to the affected tissues or cells; 3) Improving the surface properties of drugs or therapeutic macromolecules, thus, increasing their endocytosis, and promoting their delivery to the cell interior; 4) Coupling two or more drugs to achieve a synergistic treatment effect between multiple drugs; 5) Combining disease treatment drugs with imaging reagents, allowing visual imaging and disease treatment to be performed concomitantly.

The frontiers of cancer nanotechnology are constantly changing as the understanding of the biomedical properties of nanoparticles continues to expand. Since the targeting advantage of liposomes was first proposed in the 1980s, nanocarriers or reagents used to load small molecule drugs have gradually been developed diversified and applied in clinical practice (Shi et al., 2010). In particular, gold nanoparticles (AuNPs) have become a promising drug in recent years (Yang et al., 2015; Bai et al., 2020). Due to its advantages such as oxidation resistance, good biocompatibility, high density and good photoelectric properties, AuNPs have a broad application prospect in the study of electrochemical catalysis, photoelectric, physicochemical properties and other aspects. Gold is one of the least reactive metals in nature, and can be stored under natural conditions for millions of years without being destroyed by oxidation. The biological inertness of gold particles makes them an attractive candidate for drug delivery. In order to

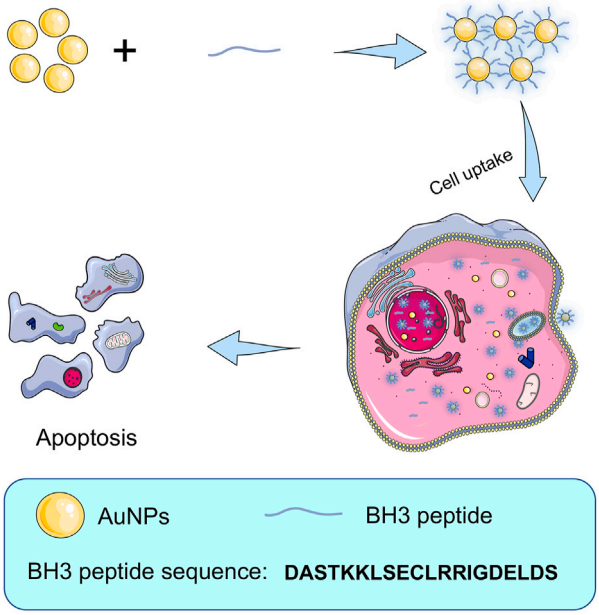

FIGURE 1
Schematic illustration of the procedure of preparing BH3@AuNPs nanoparticles for intracellular delivery of BH3 peptide and induce cell apoptosis.

prevent the toxicity and side effects that can result from aggregation of nanoparticles in the body, the surface of nanocarriers should be positively charged, hydrophilic and stable, all of which can be satisfied with gold nanoparticle technology. Many shapes of gold nanoparticles exist, including spheres (Lindley and Zhang, 2019; Hussain et al., 2021), nanoplates (Khe et al., 2012; Wang et al., 2014; Bi et al., 2018), rods (Alkilany et al., 2012; Zheng et al., 2021), nanocages (Sun et al., 2017; Nazemi et al., 2018), and more, all of which possess unique anti-tumor advantages. Studies have shown that different shapes of gold nanoparticles have a large gap in tumor imaging and therapeutic capabilities (Li and Chen, 2015; Amina and Guo, 2020), moreover, tumor absorption of gold nanospheres and gold nanorods is several times greater than that of particles with different shapes. Therefore, gold nanospheres with good dispersion and aqueous stability were selected as drug carriers in this study.

Apoptosis is a major defense mechanism against tumor development and is essential for myriad elements of immunity, development, and tissue homeostasis (Edlich, 2018). Apoptosis refers to the fragmentation of cells into vesicles (apoptotic bodies), which are then removed by phagocytosis, thus eliminating the original cell while protecting its neighbors from potentially harmful cellular contents (Kerr et al., 1972). The Bcl-2 family has long been explored for its roles in apoptosis. BH3-only protein is a

member of the Bcl-2 family, and some scholars have divided the apoptosis pathway into two types according to the different mechanisms of BH3-only. One is the relatively more common mitochondria-dependent apoptosis pathway, which uses BH3-only protein as an "activator" to induce apoptosis (Sharikova et al., 2018). The other is the recently proposed non-mitochondrial-dependent apoptotic pathway, in this pathway, after receiving the apoptotic signal, the "sensitizers" represented by BAD and BIK in BH3-only protein will replace Bax and Bak on the anti-apoptotic protein through competition (Arimochi and Morita, 2006; Manas et al., 2018). Promote the release of Bax, Bak, and so on, thereby inhibiting the function of anti-apoptotic proteins through antagonism, leading to cell apoptosis. In the process of promoting tumor apoptosis, BH3-only protein can be activated by recognizing different stimuli, and may play both initiate and regulate cell apoptosis by directly binding Bax protein or isolating Bcl-2 anti-apoptotic protein. Therefore, a single BH3 peptide (Asp-Ala-Ser-Thr-Lys-Lys-Leu-Ser-Glu-Cys-Leu-Arg-Arg-Ile-Gly-Asp-Glu-Leu-Asp-Ser) was constructed based on BH3-only protein, and the antitumor activity when delivered using gold nanoparticle systems was investigated.

In this paper, according to the advantages that the thiol group of cysteine can form a strong au-s covalent bond with gold nanoparticles, 18 nm spherical gold nanoparticles were selected as drug carrier, and BH3 peptide containing 20 amino acids was connected to the surface of gold nanoparticles to construct the drug delivery system (Figure 1). The antitumor effect and mechanism of the synthesized drug delivery system at the cellular level *in vitro* were evaluated. The results showed that BH3@AuNPs nanomaterials could induce apoptosis of A549 cancer cells, and inhibit their migration and invasion. By assessing changes in Caspase-3/-8/-9 enzyme activity, we demonstrate that BH3@AuNPs could not only promote cell apoptosis through the endogenous pathway, but that they also promoted cell apoptosis through the extracellular pathway, indicating a promising candidate for cancer treatment.

2 Materials and methods

2.1 Materials

Tetra-chloroauric acid ($HAuCl_4$), and EDTA (AR) were purchased from Sinopharm. Trisodium citrate was purchased from Sigma. Nitrogen was purchased from Changchun Ju Yang Gas Co., Monosodium phosphate (NaH_2PO_4, ACS class), sodium hydrogen phosphate (Na_2HPO_4, ACS class), sodium hydroxide (NaOH, ACS class), hydrochloric acid (HCl, ACS class), potassium bromide (KBr) were purchased from Beijing Chemical Reagent Company. Bovine serum albumin (BSA) was purchased from Sangon Biotech (Shanghai) Co., Ltd. Hydrochloric acid (HCl, AR)and anhydrous ethanol (AR) were purchased from Beijing Chemical Factory. Crystal violet was purchased from Dalian Meilun Biological Technology Co., Ltd. BH3 peptides with the sequence of DASTKKLSECLRRIGDELDS were purchased from GL Biochem (Shanghai) Ltd. Caspase-3, -8, -9 Fluorometric Assay Kits, Hoechst 33342, and Annexin V-FITC Apoptosis Detection Kits were purchased from Shanghai BestBio Company. BCA Protein Assay Kit and JC-1 Assay Kits were purchased from Beyotime Biotechnology.

2.2 Synthesis and characterization of AuNPs and BH3@AuNPs

Synthesis of gold nanoparticles (AuNPs) was based on the previously reported method (Ji et al., 2007). Briefly, 48.5 ml of water was mixed with 1.33 ml of tetrachloroauric acid solution (9.41 mM) in a three-necked flask and heated to boiling. Then 0.2 ml of sodium citrate solution (0.218 M) was quickly added under vigorous stirring. The reaction system was boiled for 10 min and then removed from heat. The system was continuously stirred for 15 min and cooled to room temperature. AuNPs were collected and measured by UV-Vis spectra and nano-size ZETA potentiometer.

To generate BH3@AuNPs 1 mg of BH3 peptide powder was dissolved in 1 ml of ultrapure water to obtain 1 mg/ml of BH3 solution. According to the desired molar ratios of 800: 1 and 1000:1 for BH3 to AuNPs, 2.74 μL and 6.86 μL BH3 solution was added to the synthesized gold nanoparticles solution, respectively. BH3 will be connected to the surface of gold nanoparticles after being left in the refrigerator at 4°C for 12 h, resulting in BH3@AuNPs-1 and BH3@AuNPs-2. The resulting of the bioactive AuNPs (BH3@AuNPs) was recovered by centrifugation (12,000 rpm, 20 min) and washed with ultrapure water three times to remove excessive peptides. The products were lyophilized by a freeze-drying machine and used for subsequent cell experiments.

2.3 Cell culture

A549 cells (passages <10; CCL-185; ATCC, Manassas, VA, United States of America) were derived from human lung adenocarcinoma cell line. They were cultured in Dulbecco's modified Eagle's medium (DMEM; Thermo Fisher Scientific, Waltham, MA, United States), and supple-mented with 20% (v/v) fetal bovine serum (FBS; Kangyuan Biology, Tianjin, China), 100 units. mL^{-1} penicillin, or 100 μg ml^{-1} streptomycin (Invitrogen, Carlsbad, CA, United States of America). The cells were incubated under a humidified atmosphere containing 5% CO_2 and 95% air at 37°C. The media were

replaced every 2 days. The cells were ready for treatment when confluence reached 75%.

2.4 Cytotoxicity assessent of AuNPs and BH3@AuNPs

A549 cells were resuscitated and cultured for (roughly three to four generations). When cell growth stabilized, they were seeded into 96-well plates at a density of 5,000 cells per well. Cells were allowed to adhere and grow in a CO_2 incubator for 12 h at 37°C. The culture medium in the 96-well plate was discarded and 20 nM AuNPs, BH3@AuNPs, or BH3 were added, while (6 parallel untreated control wells were used for each sample). Treated cells were incubated for 24 h at 37°C in a CO_2 incubator, sterile MTT solution (5 mg/ml) prepared in advance was added to each well. Cells were then restored to the incubator for 4 h, before well volumes were aspirated and 150 μL of DMSO solution was added. The mixture was shaken at a constant rate for 5 min, and the absorbance value at 492 nm was measured using a microplate reader.

2.5 Determination of drug loading of BH3@AuNPs

The loading rate of BH3 on AuNPs at different molar ratios was determined by HPLC. Set chromatographic conditions: Kromasil-C18 column (5 μm 250 × 4.6 mm), column temperature: 25°C, UV detection wavelength: 220 nm, mobile phase selected 0.02 mmol/L phosphate buffer (Na_2HPO_4 and NaH_2PO_4), sample volume = 10 μL/bottle, flow rate = 1.0 ml/min. BH3 standard solution with gradient changes (0.2 mg/ml, 0.4 mg/ml,0.6 mg/ml, 0.8 mg/ml, 1.0 mg/ml) was prepared by dissolving 1 mg BH3 powder in 1 ml ultrapure water and diluting it with ultrapure water. Eight samples with BH3 to AuNPs molar ratios of 200:1, 400:1, 600:1, 800:1, 1000:1, 2000:1, 4000:1, 6000:1 were assessed for loading rate. The peak time of BH3 was measured by HPLC and the drug loading and encapsulation rate were subsequently calculated.

2.6 Colony formation assay

A549 cells were seeded in 6-well plates at a density of 2×10^5 cells per well and grown for 12 h in a CO_2 incubator at 37°C. Different samples (control group, AuNPs group, BH3 group, BH3@AuNPs-1 group and BH3@AuNPs-2 group) were added at 20 nM and the culture medium was discarded after 24 h of co-incubation at 37°C, and cultures were continued for another 7 days. After 7 days, they were fixed with pre-cooled 70% ethanol solution for 20 min. Incubated with 0.2% crystal violet solution for 15 min, after that, the cells were carefully collected. Tumor cell growth was observed under a fluorescence inverted microscope.

2.7 Trypan blue staining

A549 cells in a stable growth state were seeded into 96-well plates at a concentration of 5×10^3 cells per well. Cells were incubated for 12 h at 37°C in a CO_2 incubator and then for an additional 24 h with the sample to be tested. Cells were digested with trypsin, the appropriate cell suspension was mixed with 0.4% trypan blue solution at a ratio of 9:1, and viable and dead cells were counted on a blood cell counting plate using a microscope within 3 min.

2.8 Hoechst-3342 staining

A549 cells in a stable growth state were seeded in 6-well plates at a density of 2×10^5 cells per well and incubated for 12 h at 37°C in a CO_2 incubator. The samples to be tested were added to the wells and incubated for 24 h. The sample solution of each well was discarded, and 70% ethanol solution precooled in advance was added for 20 min at 4°C to fix the cells. Cells were then stained with Hoechst-33342 and incubated for 20 min at room temperature before being washed three times with PBS. Tumor cell growth was observed under a fluorescence inverted microscope.

2.9 Induction of apoptosis assay

A549 cells in a stable growth state were seeded into 6-well plates at a density of 2×10^5 cells per well and subjected to different treatments. After 24 h, all cells were digested with 0.25% (w/v) trypsin and harvested. The Annexin V-FITC/PI kit dye was used for 30 min at 4°C in the dark to remove the staining solution. Cells were then suspended in PBS solution, and the fluorescence of the cells was detected and analyzed by flow cytometry. Finally, BD CellQuest Pro Software was used to assess the proportion of apoptosis present under each condition.

2.10 Wound healing assay

The effects of BH3@AuNPs-1 or BH3@AuNPs-2 on the migration ability of A549 cells were evaluated by scratch wound method. A549 cells in a stable growth state were seeded in 6-well plates at a density of 2×10^5 cells per well and cultured for 12 h at 37°C in a CO_2 incubator. Next, using a plastic pipette tip, a thin scratch was created in the cell layer, followed by treatment with different samples. At 0 and 24 h, photographs of the cells were taken.

2.11 Transwell assay

A549 cells in a stable growth state was seeded in 6-well plates at a density of 2×10^5 cells per well and incubated in a CO_2 incubator for 12 h at 37°C. After being exposed to different treatments, cells were incubated at 37°C for 24 h. Cells were digested and centrifuged, and cell precipitates were collected. Precipitates were resuspended in high glucose serum-free medium DMEM(containing 1% BSA) and seeded in Transwell membranes. At the same time, 700 μL of DMEM medium (containing 10% FBS) was added to theTranswell chamber. Plates were cultured at 37°C in a CO_2 incubator for 24 h and the Transwell chamber was removed. Cells in the lower layer of the Transwell luminal membrane were fixed with pre-cooled 70% ethanol solution at 4°C for 20 min and then washed three times with PBS. Cells in the lower layer of the Transwell chamber were then incubated with 0.2% crystal violet solution for 20 min. Cell distribution was observed under fluorescence inverted microscope.

2.12 Mitochondrial membrane potential assay

A549 cells in a stable growth state were seeded in 6-well plates at a density of 2×10^5 cells per well and cultured for 12 h at 37°C in a CO_2 incubator. The samples to be tested were incubated with the cells for 24 h at 37°C. Staining solution was added for 20 min according to JC-1 kit instructions, and then washed with PBS three times. Cell staining was observed by a fluorescence inverted microscope.

2.13 Caspase-3/-8/-9 activity assay

A549 cells in a stable growth state were seeded in a 6-well plate at a density of 2×10^5 cells per well. Cells were cultured for 12 h at 37°C in a CO_2 incubator. The samples to be tested were incubated for 24 h at 37°C in a CO_2 incubator after treatment. Cells were digested with a centrifuged and collected. Protein content of the collected cell lysates was determined according to BCA Protein Assay Kit. Extracted protein was also added to buffer and Caspase-3/-8/-9 assay substrate and incubated for 4 h at 37°C in the dark. Absorbance values at 400 nm were measured using a microplate reader.

2.14 Statistical analysis

All data are expressed as the mean ± standard deviation ($n \geq 3$), the significance of differences among groups was evaluated with a Student's t-test analysis ($^*p < 0.05$, $^{**}p < 0.01$ vs control group).

3 Results and discussion

3.1 Preparation and characterization of BH3-AuNPs

In this study, AuNPs were formed by stably reducing $HAuCl_4$ with trisodium citrate. The BH3 peptide is based on the action mechanism of Bcl-2 family proteins. Since the peptide contains a cysteine, it can be connected with gold nanoparticles by thiol coordination (Resemann et al., 2018) to form a stable delivery system. The solution of gold nanoparticles was transparent reddish-brown and uniform in color as shown in Figure 2A, and UV spectrum scanning results showed that the sample has a maximum absorption peak at 518 nm and no edge phenomenon, demonstrating successful synthesis of gold nanoparticles. TEM results are exhibited in Figure 2B, displaying that the AuNPs are spherical with a rough surface and a particle size of 18 ± 2 nm. The synthesized gold nanoparticles have good stability, size uniformity, and particle mass. At the same time, we analyzed the particle size distribution of hydrated AuNPs (Figure 2C), and found that the hydrated gold nanoparticles are 20.3 ± 0.3 nm, which is consistent with the electron microscopy results. BH3@AuNPs were generated across a gradient of relative molar ratios of BH3 to AuNPs. Assessment of loading potency of BH3 peptides on gold nanoparticles, revealed BH3@AuNPs made from ratios of 800:1 and 1000:1 BH3 to AuNPs to be the most effective, (BH3@AuNPs-1 and BH3@AuNPs-2, respectively; Figure 2E, Supplementary Figure S1; Supplementary Table S1). BH3@AuNPs-1 and BH3@AuNPs-2 both exhibited a uniform, transparent reddish-brown color, but the liquid color was slightly darker than that of AuNPs alone. The maximum absorption peak of BH3@AuNPs-1 and BH3@AuNPs-2 is at 521 nm and has no band edge (Figure 2D). Due to Au-S covalent bonding between cysteine and gold nanoparticles, the plasmon resonance absorption of gold nanoparticles is also slightly redshifted at BH3@AuNPs-1 and BH3@AuNPs-2. From these results, we can conclude that the synthesis of BH3@AuNPs-1 and BH3@AuNPs-2 samples was successful.

To further demonstrate the successful conjugation of BH3 onto AuNPs, we used infrared spectroscopy for additional characterization. As shown in Figure 2F, the infrared absorption peaks of BH3 are consistent with BH3@AuNPs-1 and BH3@AuNPs-2; however, BH3@AuNPs-1 and BH3@AuNPs-2 lack the obvious free sulfhydryl absorption peak of BH3 at 2570, demonstrating that BH3 binds to AuNPs through a sulfhydryl coordination bond. The average hydrodynamic diameter measured by dynamic light scattering (DLS) of BH3@AuNPs-1 and BH3@AuNPs-2 is 53.87 nm and 64.13 nm, respectively (Figures 2G,H). Compared with the size characterization diagram of AuNPs, the hydrated particle size of BH3@AuNPs-1 and BH3@AuNPs-2 are a bit magnified, which may be due to the sorption of BH3. In addition, the surface zeta

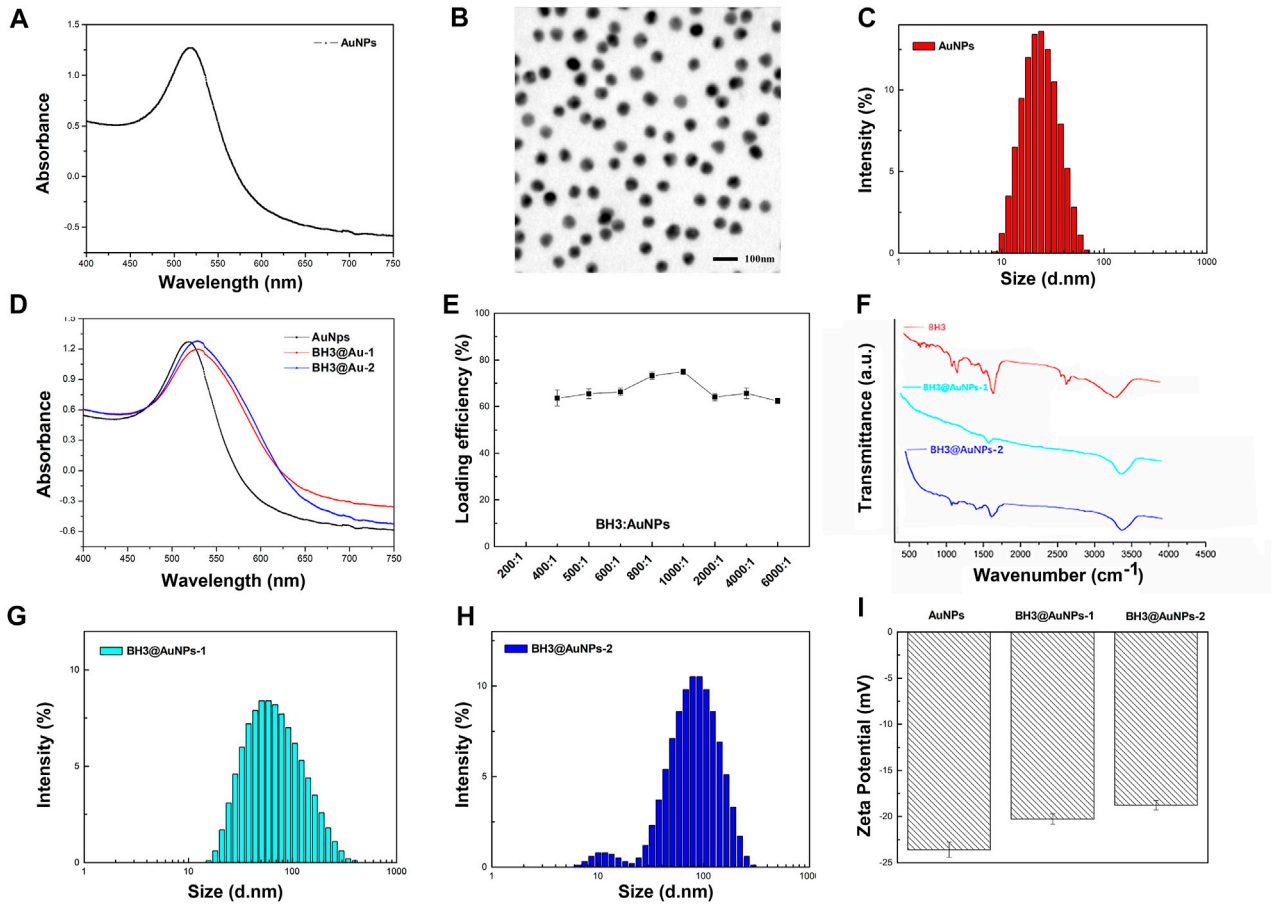

FIGURE 2
(A) UV-vis absorption spectra **(B)** TEM image of AuNPs **(C)** Average hydrodynamic diameter distribution of AuNPs **(D)** UV-vis absorption spectra of AuNPs, BH3@AuNPs-1, and BH3@AuNPs-2 **(E)** Loading efficiency of different relative mass ratios of BH3 and AuNPs **(F)** FT-IR spectra of BH3, BH3@AuNPs-1, and BH3@AuNPs-2 **(G)** Average hydrodynamic diameter distribution of BH3@AuNPs-1 and **(H)** BH3@AuNPs-2 **(I)** Zeta potential values of AuNPs, BH3@AuNPs-1, and BH3@AuNPs-2.

potential readings changed from negative (−23.4 mV) to −20.3 mV and −19.9 mV after the modification of the BH3 component (Figure 2I), further indicating that BH3@AuNPs-1 and BH3@AuNPs-2 were synthesized successfully.

3.2 Cytotoxicity analysis and Hoechst staining experiment

To verify the vector toxicity of gold nanoparticles and the inhibitory effect of BH3@AuNPs on cancer cells, an MTT assay was performed. As presented in Figure 3A, the survival rate of A549 cells treated with AuNPs at four different concentrations (5, 10, 15, and 20 nM) showed almost no toxic effect and A549 cells grew well after treatment with AuNPs. Cell viability under these conditions was above 90%, which was deemed sufficient for their use as a drug transport carrier for the subsequent experiment. As evident from Figure 3B, in comparison with the control group AuNPs group and BH3 peptide group, cell viability was remarkably lower in BH3@AuNPs-1 or BH3@AuNPs-2 treatment group with the same drug concentration as free BH3, owing to the sustained drug release effect of BH3@AuNPs. This decrease in cell viability was attributed to the effective delivery of BH3 peptides into cells by gold nanoparticles, while the BH3 peptides alone did not demonstrate the same degree of cellular toxicity, presumably due to its relatively large molecular mass preventing its passage through the cell membrane. We validated these results by assessing the survival of A549 cells treated with AuNPs, BH3 peptide, BH3@AuNPs-1, and BH3@AuNPs-2 for 24 h using a Trypan blue staining assay. The ratio of live/dead cells was counted under the microscope with a blood count plate, and the viability of A549 cells treated under each condition was calculated. As shown in Figure 3C, similar experimental results

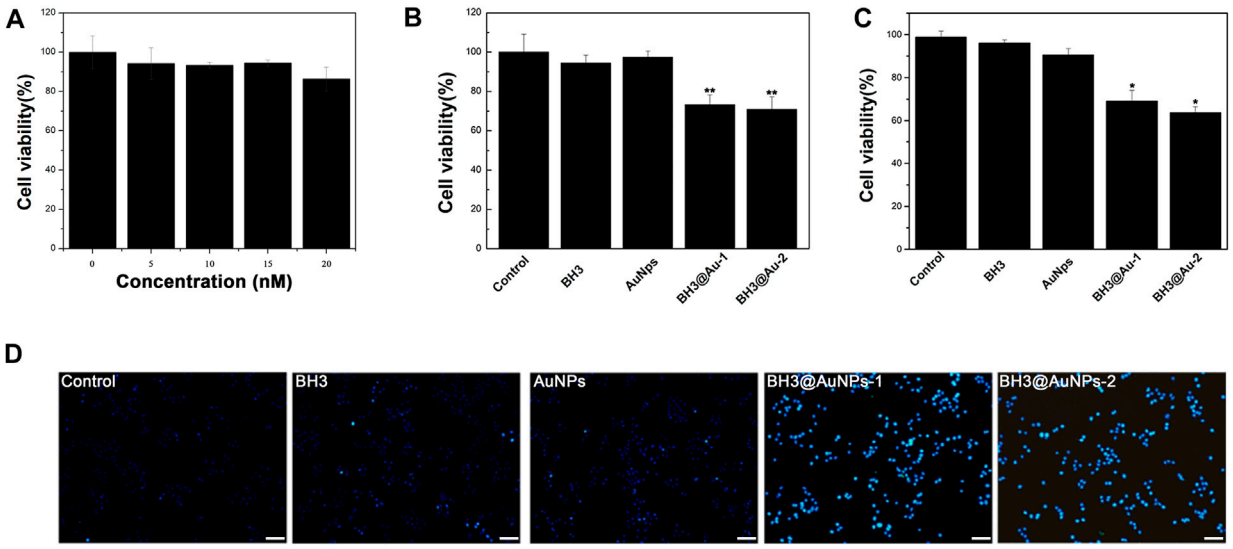

FIGURE 3
(A) Viability of A549 cells treated with different concentrations of gold nanoparticles and **(B)** BH3 peptide, AuNPs, BH3@AuNPs-1 and BH3@AuNPs-2 for 24 h by MTT **(C)** Viability of A549 cells treated with BH3 peptide, AuNPs, BH3@AuNPs-1, and BH3@AuNPs-2 calculated by trypan blue staining. Data are shown as mean ± SD (n = 3) **(D)** Hoechst 33,342 staining of A549 cells treated with different materials observed by fluorescence microscopy. The scale bar is 100 μm. Data are presented as mean value ±SD of triplicate experiments. *$p < 0.05$; **$p < 0.01$.

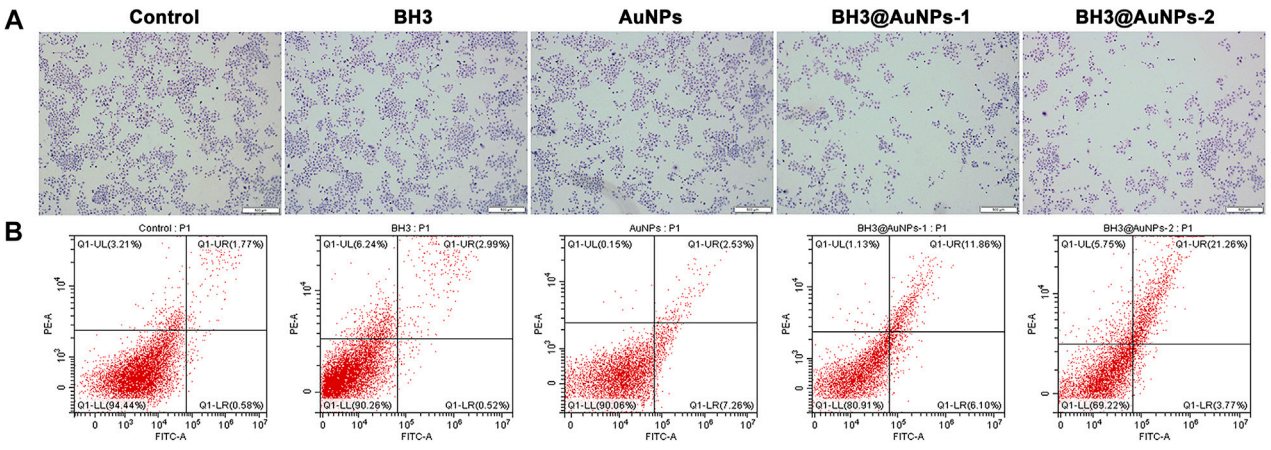

FIGURE 4
(A) The colony formation ability of A549 cells treated with different samples for 24 h was observed by fluorescence microscopy (Scale bar: 500 μm) **(B)** Cell apoptosis induction by BH3, AuNPs, BH3@AuNPs-l, and BH3@AuNPs-2 using Annexin V/PI protocol.

were obtained, further confirming the cytotoxic effect of BH3@AuNPs on A549 cells.

In order to more clearly assess the effect of BH3 peptide on cells, we used Hoechst 33342 fluorescent dye for nuclear staining, and detection of apoptosis. A miniscule amount of it can enter the normal cell membrane, staining it with dark blue color. The enhanced membrane permeability of apoptotic cells and structural changes of chromosomal DNA make the dye more capable of binding to DNA in such cells, resulting in bright blue fluorescence intensity in apoptotic cells than in normal cells. Notably, cells treated with BH3@AuNPs-1 and BH3@AuNPs-2 exhibited intense blue nuclear fluorescence (Figure 3D, Supplementary Figure S2) consistent with previous experimental results of the cytotoxicity of these formulations. In sum, these data together demonstrate that this new type of peptide can induce apoptosis in cancer cells

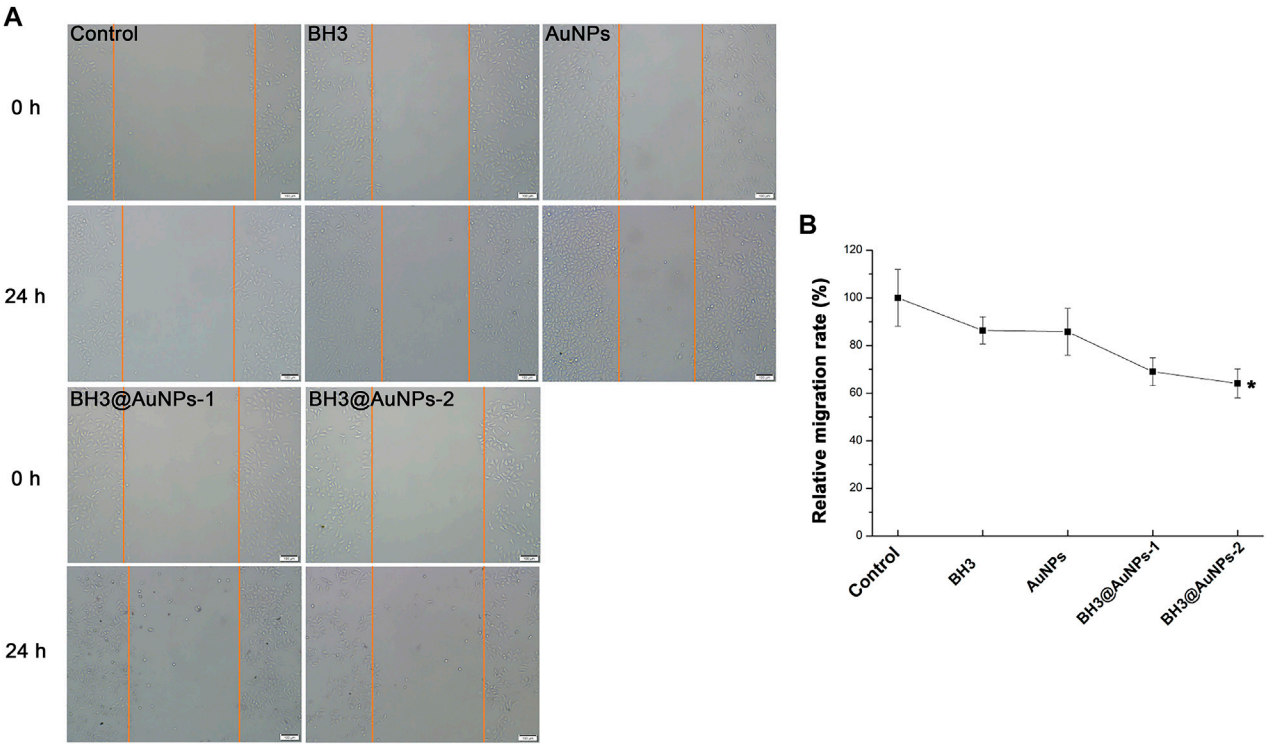

FIGURE 5
(A) Wound healing and **(B)** quantitative analysis (24 h) of A549 cells treated with different samples at 0 h and 24 h. The scale bar is 100 μm. Data are presented as mean value ±SD of triplicate experiments. *$p < 0.05$.

and may represent a promising candidate for tumor therapy in the future.

3.3 Colony formation and cell apoptosis experiments

A colony formation assay was used to observe the growth distribution of A549 cells treated with BH3 peptide, AuNPs, BH3@AuNPs-1, and BH3@AuNPs-2 for 24 h after propagation *in vitro* for more than six generations, as shown in Figure 4A. We found that the cell growth distribution of the BH3 peptide and AuNPs groups were similar to that of the control group, with the formation of larger, single cell-centered colonies, and a healthy cell growth rate. However, in cells treated with BH3@AuNPs-l or BH3@AuNPs-2, only a few single cell-centered colonies were formed, cell colonies were smaller and cell growth was slower. These results, further demonstrated the inhibitory effect of BH3@AuNPs-l and BH3@AuNPs-2 on tumor cell proliferation also highlighting their capacity to significantly reduce the ability of cells to form colonies. To further test the apoptosis-inducing effect on A549 cells, flow cytometry was used to detect apoptosis after treatment with BH3 peptide, AuNPs, BH3@AuNPs-l, BH3@AuNPs-2 (Figure 4B). Similar apoptotic ratio was obtained while cells treated with BH3 peptide (3.51%), gold nanoparticles (9.79%) to control (2.35%), suggesting that cells treated with neither BH3 peptide alone nor AuNPs can induce apoptosis. Remarkably, cells treated with BH3@AuNPs-l or BH3@AuNPs-2 showed it effectively initiates early-stage apoptosis with the apoptotic ratio of 17% and 24%, respectively. These results proved that BH3 peptide carried by gold nanoparticles can effectively inhibit the growth of tumor cells and promote apoptosis.

3.4 Evaluation of the ability to inhibit cell migration and infiltration

For cancer patients, surgical resection of the tumor represents one of the most commonly used treatment methods, but the probability of disease recurrence due to tumor metastasis is quite large after these procedures (Lin et al., 2019; Zhang et al., 2020). Therefore, it is necessary to evaluate whether gold nanoparticles loaded with BH3 peptides can effectively regulate the migration and invasion of tumor cells. First, we analyzed the migration ability of tumor cells after treatment *via* wound healing assay. As shown in Figures 5A,B, scratches in wells containing cells treated with AuNPs and BH3 healed rapidly, indicating that

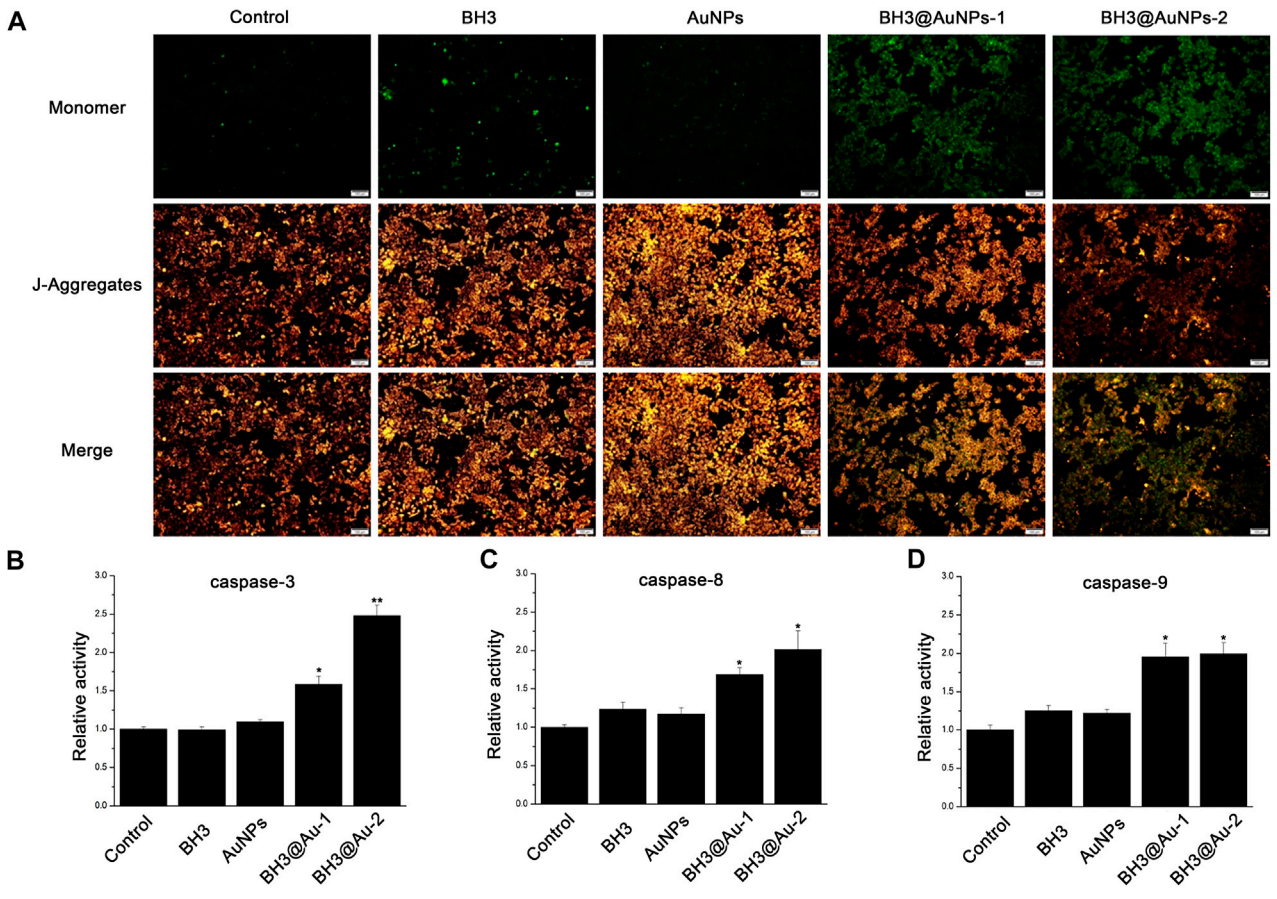

FIGURE 6
(A) Mitochondrial membrane potential after treatment of A549 cells with different experimental groups (Scale bar: 100 μm) **(B)** Relative activities of intracellular Caspase-3, Caspase-8 **(C)**, and Caspase-9 **(D)** in A549 cells treated with BH3, AuNPs, BH3@AuNPs-1, and BH3@AuNPs-2. Data are presented as mean value ±SD of triplicate experiments. *$p < 0.05$; **$p < 0.01$.

neither of the two materials effectively inhibited cell migration. Remarkably, when cells were treated with BH3@AuNPs-1 or BH3@AuNPs-2, the scratches did not heal effectively, and were almost unchanged after 24 h. This result suggested that BH3 peptide can effectively inhibit tumor migration after being delivered to cells by gold nanoparticles. In addition, a Transwell assay was used to verify whether BH3 delivery could effectively inhibit tumor cell infiltration. A549 cells treated with different nanocomplexes were seeded in transwell membranes and cultured for 24 h, and the cells infiltrating through the transwell into the lower layer were observed and analyzed by microscopy (Supplementary Figure S3). Untreated tumor cells effectively migrated to the other side of the transwell polycarbonate membrane through small holes, indicating a strong ability to infiltrate. Similarly, cells treated with free BH3 and AuNPs rapidly infiltrated through the transwell membrane into the lower layer. In contrast, cells treated with BH3@AuNPs-1 or BH3@AuNPs-2 showed significantly less infiltration, indicating that only a small number of cells could penetrate the transwell membrane after these treatments. This further supported the conclusion that BH3 peptides delivered to cells by AuNPs can effectively inhibit tumor cell infiltration metastasis.

3.5 Antitumor mechanism of BH3@AuNPs

Since the BH3 domain is involved in promoting apoptosis in Bcl-2 family proteins, caspase-3,-8,-9 activities were assessed to explore the pro-apoptotic mechanism of BH3 peptides based on the caspase pathways of apoptosis. As shown in Figures 6B–D, activities of the caspase-3,8,9 enzymes after treatment with BH3 peptide or AuNPs alone were consistent with those of the control group, while cells treated with BH3@AuNPs-1 or BH3@AuNPs-2 showed significantly up-regulated caspase -3,-8,-9 activity, indicating that the three enzymes were activated in the sample group. Two apoptosis pathways have been elucidated to date, one being the mitochondria-mediated apoptosis pathway involving caspase-9 (also known as endogenous apoptosis pathway), and

the other being the death receptor-mediated apoptosis pathway involving caspase-8 (also known as exogenous apoptosis pathway). After the delivery of BH3 peptide *via* the gold nanoparticles, cells simultaneously activated both the mitochondrial apoptosis pathway as well as the death receptor apoptosis pathway, resulting in apoptosis. After initiation of the mitochondrial apoptosis pathway, the membrane potential of intracellular mitochondria is known to decrease, therefore, we used the fluorescent probe JC-1 to assess the change in mitochondrial membrane potential after treatment (Figure 6A). Compared with AuNPs alone, cells showed more green fluorescence after treatment with BH3@AuNPs, indicating that the mitochondrial membrane potential had decreased significantly. This phenomenon once again verified that AuNPs loaded with BH3 peptide can effectively initiate apoptosis through the endogenous apoptosis pathway.

4 Conclusion

In summary, a BH3 peptide of 20 amino acids was successfully ligated to 18 nm gold nanoparticles *via* Au-S coordination bond, and the effect of *in vitro* treatment of lung cancer cells was assessed. Compared with gold nanoparticles or BH3 peptides alone, BH3@AuNPs showed relatively high drug loading efficiency. BH3 peptide was effectively delivered by gold nanoparticles into the cell, achieving activation of both endogenous and exogenous apoptosis pathways and inhibiting cell growth and migration. This approach addresses the challenges associated with treatments using BH3 peptides alone, such as poor stability of antiprotease hydrolysis, and low endosomal escape rate of BH3 peptide, and provides a new approach for the subsequent study of BH3-mimic peptide drugs.

Data availability statement

The original contributions presented in the study are included in the article/Supplementary Material, further inquiries can be directed to the corresponding authors.

Author contributions

XZ and QY: writing the manuscript, conceptualization, investigation, and editing; JW: writing the manuscript; LX and YG: conceptualization, investigation, funding acquisition, supervision, and review writing and editing.

Funding

This work was supported by grants from the National Natural Science Foundation of China (82172100) and the Project of Science and Technology Department of Jilin Province, China (No.20170204027NY, 20200801015GH, 20200404100YY, 20210402039GH, 20220101299JC).

Conflict of interest

The authors declare that the research was conducted in the absence of any commercial or financial relationships that could be construed as a potential conflict of interest.

Publisher's note

All claims expressed in this article are solely those of the authors and do not necessarily represent those of their affiliated organizations, or those of the publisher, the editors and the reviewers. Any product that may be evaluated in this article, or claim that may be made by its manufacturer, is not guaranteed or endorsed by the publisher.

Supplementary material

The Supplementary Material for this article can be found online at: https://www.frontiersin.org/articles/10.3389/fmats.2022.1099997/full#supplementary-material

References

Alkilany, A. M., Thompson, L. B., Boulos, S. P., Sisco, P. N., and Murphy, C. J. (2012). Gold nanorods: Their potential for photothermal therapeutics and drug delivery, tempered by the complexity of their biological interactions. *Adv. Drug Deliv. Rev.* 64 (2), 190–199. doi:10.1016/j.addr.2011.03.005

Allemani, C., Matsuda, T., Di Carlo, V., Harewood, R., Matz, M., Niksic, M., et al. (2018). Global surveillance of trends in cancer survival 2000-14 (CONCORD-3): Analysis of individual records for 37 513 025 patients diagnosed with one of 18 cancers from 322 population-based registries in 71 countries. *Lancet* 391 (10125), 1023–1075. doi:10.1016/s0140-6736(17)33326-3

Amina, S. J., and Guo, B. (2020). <p>A review on the synthesis and functionalization of gold nanoparticles as a drug delivery vehicle</p>. *Int. J. Nanomedicine* 15, 9823–9857. doi:10.2147/ijn.S279094

Arimochi, H., and Morita, K. (2006). Characterization of cytotoxic actions of tricyclic antidepressants on human HT29 colon carcinoma cells. *Eur. J. Pharmacol.* 541 (1-2), 17–23. doi:10.1016/j.ejphar.2006.04.053

Bai, X., Wang, Y. Y., Song, Z. Y., Feng, Y. M., Chen, Y. Y., Zhang, D. Y., et al. (2020). The basic properties of gold nanoparticles and their applications in tumor diagnosis and treatment. *Int. J. Mol. Sci.* 21 (7), 2480. doi:10.3390/ijms21072480

Bi, Z.-F., Yang, M., and Shang, G.-Y. (2018). Optical polarization response at gold nanosheet edges probed by scanning near-field optical microscopy. *Chin. Phys. B* 27 (8), 087801. doi:10.1088/1674-1056/27/8/087801

Chen, H. B., Gu, Z. J., An, H. W., Chen, C. Y., Chen, J., Cui, R., et al. (2018). Precise nanomedicine for intelligent therapy of cancer. *Sci. China Chem.* 61 (12), 1503–1552. doi:10.1007/s11426-018-9397-5

Edlich, F. (2018). BCL-2 proteins and apoptosis: Recent insights and unknowns. *Biochem. Biophysical Res. Commun.* 500 (1), 26–34. doi:10.1016/j.bbrc.2017.06.190

Etheridge, M. L., Campbell, S. A., Erdman, A. G., Haynes, C. L., Wolf, S. M., and McCullough, J. (2013). The big picture on nanomedicine: The state of investigational and approved nanomedicine products. *Nanomedicine Nanotechnol. Biol. Med.* 9 (1), 1–14. doi:10.1016/j.nano.2012.05.013

Hussain, N., Pu, H., and Sun, D.-W. (2021). Core size optimized silver coated gold nanoparticles for rapid screening of tricyclazole and thiram residues in pear extracts using SERS. *Food Chem.* 350, 129025. doi:10.1016/j.foodchem.2021.129025

Ji, X. H., Song, X. N., Li, J., Bai, Y. B., Yang, W. S., and Peng, X. G. (2007). Size control of gold nanocrystals in citrate reduction: The third role of citrate. *J. Am. Chem. Soc.* 129 (45), 13939–13948. doi:10.1021/ja074447k

Kerr, J. F., Wyllie, A. H., and Currie, A. R. (1972). Apoptosis: A basic biological phenomenon with wide-ranging implications in tissue kinetics. *Br. J. Cancer* 26 (4), 239–257. doi:10.1038/bjc.1972.33

Khe, C., Aziz, A., and Lockman, Z. (2012). Synthesis of cobalt/gold bimetallic particles with porous flake-like nanostructures and their magnetic properties. *Nanosci. Nanotechnol. Lett.* 4 (7), 687–692. doi:10.1166/nnl.2012.1390

Lee, Y. T., Tan, Y. J., and Oon, C. E. (2018). Molecular targeted therapy: Treating cancer with specificity. *Eur. J. Pharmacol.* 834, 188–196. doi:10.1016/j.ejphar.2018.07.034

Li, J. C., Luo, Y., and Pu, K. Y. (2021). Electromagnetic nanomedicines for combinational cancer immunotherapy. *Angew. Chem. Int. Ed.* 60 (23), 12682–12705. doi:10.1002/anie.202008386

Li, W. W., and Chen, X. Y. (2015). Gold nanoparticles for photoacoustic imaging. *Nanomedicine* 10 (2), 299–320. doi:10.2217/nnm.14.169

Lin, Y., Xu, J., and Lan, H. (2019). Tumor-associated macrophages in tumor metastasis: Biological roles and clinical therapeutic applications. *J. Hematol. Oncol.* 12, 76. doi:10.1186/s13045-019-0760-3

Lindley, S. A., and Zhang, J. Z. (2019). Bumpy hollow gold nanospheres for theranostic applications: Effect of surface morphology on photothermal conversion efficiency. *ACS Appl. Nano Mat.* 2 (2), 1072–1081. doi:10.1021/acsanm.8b02331

Ling, X., Tu, J. S., Wang, J. Q., Shajii, A., Kong, N., Feng, C., et al. (2019). Glutathione-Responsive prodrug nanoparticles for effective drug delivery and cancer therapy. *Acs Nano* 13 (1), 357–370. doi:10.1021/acsnano.8b06400

Manas, A., Davis, A., Lamerand, S., and Xiang, J. (2018). Detection of pro-apoptotic BaxΔ2 proteins in the human cerebellum. *Histochem. Cell Biol.* 150 (1), 77–82. doi:10.1007/s00418-018-1669-6

Nazemi, M., Panikkanvalappil, S. R., and El-Sayed, M. A. (2018). Enhancing the rate of electrochemical nitrogen reduction reaction for ammonia synthesis under ambient conditions using hollow gold nanocages. *Nano Energy* 49, 316–323. doi:10.1016/j.nanoen.2018.04.039

Resemann, A., Liu-Shin, L., Tremintin, G., Malhotra, A., Fung, A., Wang, F., et al. (2018). Rapid, automated characterization of disulfide bond scrambling and IgG2 isoform determination. *Mabs* 10 (8), 1200–1213. doi:10.1080/19420862.2018.1512328

Sharikova, A. V., Quaye, E., Park, J. Y., Maloney, M. C., Desta, H., Thiyagarajan, R., et al. (2018). Methamphetamine induces apoptosis of microglia via the intrinsic mitochondrial-dependent pathway. *J. Neuroimmune Pharmacol.* 13 (3), 396–411. doi:10.1007/s11481-018-9787-4

Shi, J., Votruba, A. R., Farokhzad, O. C., and Langer, R. (2010). Nanotechnology in drug delivery and tissue engineering: From discovery to applications. *Nano Lett.* 10 (9), 3223–3230. doi:10.1021/nl102184c

Sun, H., Su, J., Meng, Q., Yin, Q., Chen, L., Gu, W., et al. (2017). Cancer cell membrane-coated gold nanocages with hyperthermia-triggered drug release and homotypic target inhibit growth and metastasis of breast cancer. *Adv. Funct. Mat.* 27 (3), 1604300. doi:10.1002/adfm.201604300

Wang, C., Du, J., Wang, H., Zou, C. e., Jiang, F., Yang, P., et al. (2014). A facile electrochemical sensor based on reduced graphene oxide and Au nanoplates modified glassy carbon electrode for simultaneous detection of ascorbic acid, dopamine and uric acid. *Sensors Actuators B Chem.* 204, 302–309. doi:10.1016/j.snb.2014.07.077

Wang, Y. L., Sun, S. Y., Zhang, Z. Y., and Shi, D. L. (2018). Nanomaterials for cancer precision medicine. *Adv. Mater.* 30 (17). doi:10.1002/adma.201705660

Xu, C. F., Li, D. D., Cao, Z. T., Xiong, M. H., Yang, X. Z., and Wang, J. (2019). Facile hydrophobization of siRNA with anticancer drug for non-cationic nanocarrier-mediated systemic delivery. *Nano Lett.* 19 (4), 2688–2693. doi:10.1021/acs.nanolett.9b00657

Yahya, E. B., and Alqadhi, A. M. (2021). Recent trends in cancer therapy: A review on the current state of gene delivery. *Life Sci.* 269, 119087. doi:10.1016/j.lfs.2021.119087

Yang, X., Yang, M., Pang, B., Vara, M., and Xia, Y. (2015). Gold nanomaterials at work in biomedicine. *Chem. Rev.* 115 (19), 10410–10488. doi:10.1021/acs.chemrev.5b00193

Zhang, H., and Liu, P. (2019). Bio-inspired keratin-based core-crosslinked micelles for pH and reduction dual-responsive triggered DOX delivery. *Int. J. Biol. Macromol.* 123, 1150–1156. doi:10.1016/j.ijbiomac.2018.11.178

Zhang, W., Wang, F., Hu, C., Zhou, Y., Gao, H., and Hu, J. (2020). The progress and perspective of nanoparticle-enabled tumor metastasis treatment. *Acta Pharm. Sin. B* 10 (11), 2037–2053. doi:10.1016/j.apsb.2020.07.013

Zheng, J., Cheng, X., Zhang, H., Bai, X., Ai, R., Shao, L., et al. (2021). Gold nanorods: The most versatile plasmonic nanoparticles. *Chem. Rev.* 121 (21), 13342–13453. doi:10.1021/acs.chemrev.1c00422

Zou, L. L., Wang, H., He, B., Zeng, L. J., Tan, T., Cao, H. Q., et al. (2016). Current approaches of photothermal therapy in treating cancer metastasis with nanotherapeutics. *Theranostics* 6 (6), 762–772. doi:10.7150/thno.14988